

Multifunctional metal-doped carbon nanocapsules

Stanislav R. Stoyanov^{1,2,a)} and Petr Král^{1,b)}¹*Department of Chemistry, University of Illinois at Chicago, Chicago, Illinois 60607, USA*²*Department of Mechanical Engineering, University of Alberta, and National Institute for Nanotechnology, National Research Council of Canada, Edmonton, Alberta, T6G 2M9, Canada*

(Received 27 August 2008; accepted 28 October 2008; published online 15 December 2008)

We present an *ab initio* study of carbon fullerenes, such as C₂₀, C₃₆, C₅₆, C₆₀, and C₆₈, that are substitutionally doped with *transition metals* coordinated to several nitrogen atoms. These capsules with porphyrinlike metal sites have remarkable electronic and spin polarizations. Additional doping by boron increases their highest occupied molecular orbital–lowest unoccupied molecular orbital gap, stabilizes their electronic structure, and causes their ground states to have higher spin multiplicity, where the spin density is spread over the capsule. These capsules could be applied in molecular electronics, catalysis, light harvesting, and nanomechanics. © 2008 American Institute of Physics. [DOI: 10.1063/1.3033758]

I. INTRODUCTION

Carbon fullerenes,¹ nanotubes,² or nanocones³ have numerous potential applications due to their unique physical and chemical properties.⁴ Similarly, BN nanotubes⁵ and nanocapsules⁶ are becoming of a large relevance, for example, as photoactive and piezoelectric materials.⁷ When functionalized by physisorption⁸ and covalent bonding,⁹ these systems can also be used in sensing and controlling of biomolecules¹⁰ or carrying of drugs.¹¹ Their spectrum of applications could be further extended if universal binding sites are introduced into these structures allowing stable chemical, electronic, and mechanical connectivity to different types of ligands.

Ewels and Glerup¹² discussed several possible atomic configurations for the N doping of carbon nanostructures. We have shown that transition metal atoms coordinated to three and four N atoms could be integrated into carbon nanocones by substituting a similar number of C atoms.¹³ In this way, *metallic binding sites* can be formed in the nanostructures that can be further functionalized. External homogenous electric field could also be used for controlled attachment and release of metal ions at the tips of metal-doped carbon nanocones and carbon nanotubes (CNTs).¹⁴ The N atoms bonded to two to three C atoms in CNTs were observed experimentally,¹⁵ where the N atoms form three stable pyridinelike substitution sites and vacancies in the CNT walls. Dodelet and co-workers¹⁶ found that an oxygen reduction reaction (ORR) catalyst prepared by pyrolysis of Fe(II) acetate supported over carbon in the presence of ammonia can achieve good activity. The increased ORR activity of this catalyst has been attributed to the active sites FeN₂–C and FeN₄–C, where Fe is coordinated to two or four pyridinic or pyrrolic N atoms embedded in the conjugated carbon plane at elevated temperature. Recently, FeN₄ sites embedded in aligned CNTs were synthesized by chemical vapor deposi-

tion process.¹⁷ Reaction studies showed that these metal and nitrogen doped CNTs are catalytically active toward the ORR and stable in acidic electrolyte, mimicking the cathode environment of polymer electrolyte fuel cells.^{17,18} The doping mode of a transition metal atom coordinated to four N atoms is very similar to that of our cone and CNT structures.^{13,14}

Carbon capsules doped by metals and functionalized by ligands might have many interesting applications. The most studied fullerene C₆₀ (Ref. 4) can be chemically activated upon introduction of heteroatoms, such as Si,¹⁹ B, and N.^{20,21} We might try to build the “periodic table” of doped nanocapsules by starting from the smallest observed fullerene, C₂₀. It contains 12 pentagonal rings and is highly strained because of the extreme pyramidalization of its double bonds. Its stability arises from electron correlations²² and might be controlled by doping, as shown by Alder *et al.*²³ The C₁₂P₈ fullerene can be particularly stable, whereas C₁₂N₈ should be very unstable. Pattanayak *et al.*²⁴ investigated BN doping of small (C₂₀–C₄₀) fullerenes and found that the BN pair would preferably replace a short C–C bond located at the hexagon-pentagon junction due to the polarization of the system. A number of metal-doped analogs of C₂₀, called metalcarba-drenes (metcars) that contain eight Ti, V, or Mo atoms, were also synthesized by Castleman and co-workers and others.^{25–28} In particular, Ti₈C₁₂⁺ is a promising catalyst for hydrodesulfurization of oils because of its strong interaction with thiophene.²⁹ Theoretical predictions also show that C₂₀ has a remarkable activity toward the addition of alkenes,²⁸ while C₃₆ is highly reactive and has a strong tendency to form intermolecular covalent bonds. The applications of fullerenes in electronics have also been explored. C₂₀ and C₃₆ have been encapsulated in semiconducting CNTs,³⁰ leading to various peapod structures. The insertion of different types of metallofullerenes into CNTs, such as Gd encapsulated in C₈₂,³¹ could allow for their complex band-gap engineering.³²

We study by *ab initio* methods metal-nitrogen-doped carbon nanocapsules. The systems are designed like substi-

^{a)}Electronic mail: stoyanov@ualberta.ca.

^{b)}Electronic mail: pkrál@uic.edu.

tionally doped fullerenes merged with nanocones. The formed metal doping sites offer superior binding and functionalization opportunities with potential applications in electronic, photonic, and nanomechanical devices.

II. COMPUTATIONAL TECHNIQUE

We describe the structure and electronic properties of the complexes by using density functional theory (DFT) that has proven to be a powerful tool for investigation of transition metal complexes.³³ The geometry and electronic structure optimization of the complexes is performed by using the B3LYP exchange-correlation functional incorporated in the GAUSSIAN 03 software package.³⁴ The all-electron triple- ζ 6-311G** basis set is used for Ni, Fe, S, B, C, N, and H atoms.³⁵ For the valence shell of Th, Os, Re, Ce, and Ru atoms, we use the Stuttgart–Dresden (SDD) basis set and for the core electrons, we use the SDD effective core potentials.³⁶ For all structures we apply pruned integration grid that has 75 radial and 302 angular points per shell. For comparison, we also perform optimizations of these structures with the Amsterdam density functional (ADF),³⁷ where we use the BLYP exchange-correlation functional and the generalized gradient approximation. For all atoms, we utilize the triple- ζ basis set that includes polarization functions on H atoms (TZP).

III. NANOCAPSULE DESIGN

In Fig. 1, we present DFT-optimized geometries of a series of Ni-, N-, and B-doped nanocapsules that are structurally related to C (Ref. 1) and BN (Ref. 38) fullerenes, as well as to Ni(II) and N doped carbon nanocones.¹³ These polymetallic capsules are obtained as follows.

- (1) The smallest metalocapsule 1 ($C_8N_8Ni_2$) is obtained from the I_h isomer of C_{20} in whose tips two pairs of fused 5–5 rings are substituted with two pairs of 4–4 rings. In Fig. 2 (left), we show part of the surface of carbon fullerene C_{20} that contains fused 5–5 rings. In this structure, two adjacent C atoms are substituted with a single Ni atom. Also, all four C atoms adjacent to Ni are substituted with N atoms to yield a NiN_4 moiety that contains 4–4 rings. In capsule 1, the N atoms are part of four pyrrolic rings. Bimetallic capsule 1 can also be designed from two doubly fused biimidazole ligands. Its structure is similar to some photochemically active Ru(II) complexes.³⁹ The eight N atom substitution mode of C_{20} considered by Alder *et al.*²³ is the same as in capsule 1.
- (2) Nanocapsule 2 ($C_{24}N_8Ni_2$) is obtained from the D_{2d} isomer of C_{36} , where two pairs of fused 6–6 rings are substituted with two pairs of 5–5 rings. In Fig. 2 (right), we show a part of the C_{36} fullerene surface that contains fused 6–6 rings. In this structure, two adjacent C atoms at the 6–6 ring fusion area are substituted with a single Ni atom. Also, all four C atoms adjacent to Ni are substituted with N atoms to yield a NiN_4 moiety that contains 5–5 rings. In nanocapsule 2, the four N atoms belong to four pyrrolic rings. This capsule can

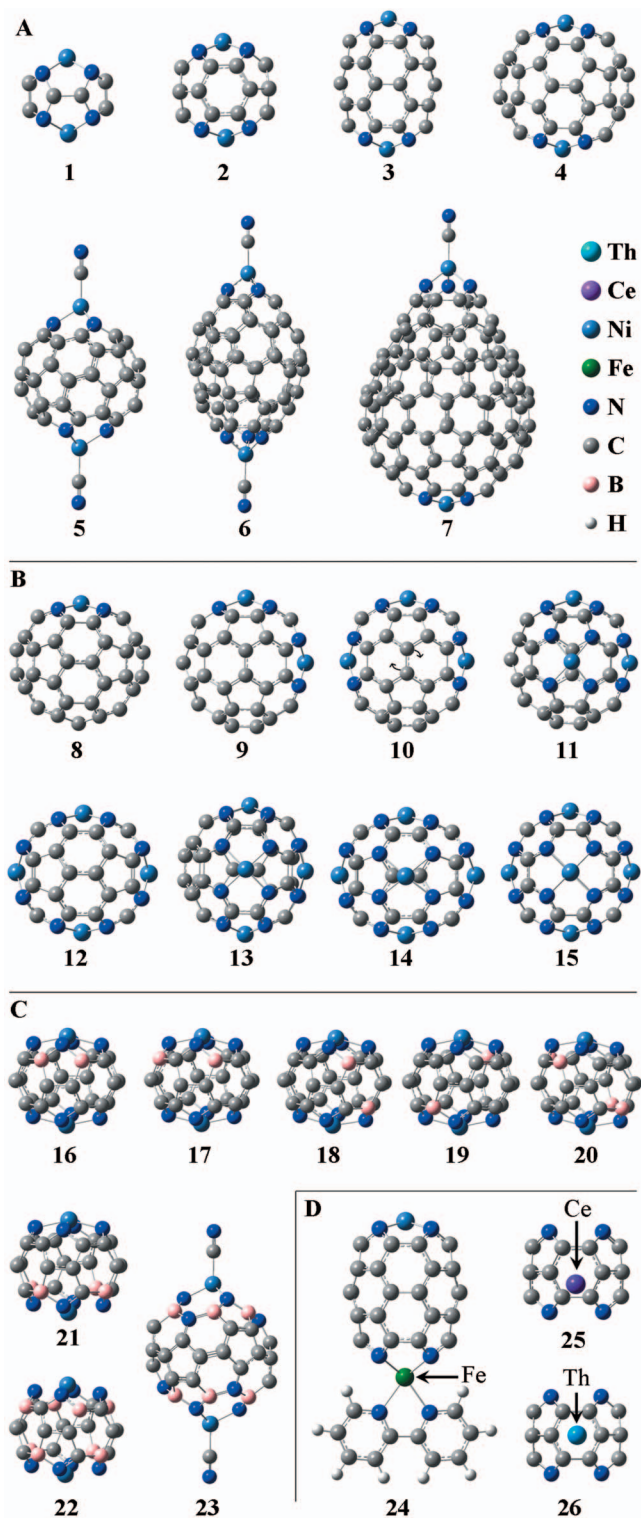


FIG. 1. (Color) Metal-doped carbon nanocapsules.

- also be designed by fusion of two metal-tipped nanocones¹³ and extended by addition of CNT segments. Capsule 3 ($C_{40}N_8Ni_2$) is obtained by insertion of a (4,4) CNT unit cell into capsule 2.
- (3) Nanocapsule 4 ($C_{48}N_8Ni_2$) is obtained from the I_h isomer of C_{60} , where two pairs of fused 6–6 rings located at the opposite sides of the buckyball are substituted with two pairs of 5–5 rings [Fig. 2 (right)]. In 4, the N

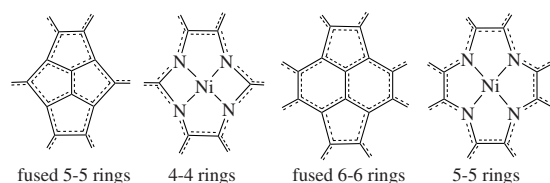


FIG. 2. Metal and nitrogen doping patterns for capsules 1 (left) and 2–4 (right).

atoms belong to pyridinic rings. This structure differs from C_{60} in *eight* C to N substitutions and *two* closures with Ni atoms instead of two C atoms. It can also be designed by fusion of two 120° cones³ along the “zig-zag” rim.¹³

- (4) Nanocapsule 5 ($C_{50}N_8Ni_2$) is obtained from a 180° cone frustrated by three pyrrole defects. The all-carbon analog of nanocapsule 5, C_{56} , would be highly strained due to two pairs of fused six-membered rings that share one C atom. Nanocapsule 6 ($C_{62}N_8Ni_2$) is also obtained from a 180° cone, and it is analogous to the D_3 isomer of C_{68} .²¹ Capsules 5 and 6 contain two Ni atoms that form four-coordinate (approximate tetrahedral) complexes. The tetrahedral coordination is completed by the addition of a CN^- ligand. Metal-doped 180° cones can also form octahedral complexes.¹³
- (5) Nanocapsule 7 ($C_{119}N_8Ni_2$) is obtained from 180° (top) and 120° bottom cones³ fused as in (12,0) CNT. The top portion differs from the carbon 180° cone in three N–C substitutions and a Ni atom at the tip instead of a C atom. The bottom portion differs from the carbon 120° cone in four N–C substitutions and a Ni atom at the tip instead of two C atoms.
- (6) Nanocapsules 8–15 are obtained from C_{60} and contain one to six Ni atom closures, designed in analogy to those in capsule 4. The molecular formulas of capsules 8, 14, and 15 are $C_{54}N_4Ni$, $C_{30}N_{20}Ni_5$, and $C_{24}N_{24}Ni_6$, respectively. In addition, we consider the isomer of 10 (listed as 10') obtained by Stone–Wales rearrangement, as shown by the arrows. The capsules 10, 10', and 11 ($C_{42}N_{12}Ni_3$) are isoelectronic structural isomers. Capsule pairs 9 and 4 ($C_{48}N_8Ni_2$) as well as 12 and 13 ($C_{36}N_{16}Ni_4$) are also isoelectronic structural isomers.
- (7) The capsules can be further doped with B atoms, as shown in 16–23. Isoelectronic capsules 16–19 ($B_2C_{22}N_8Ni_2$) are obtained by two B-atom dopings of capsule 2. Isoelectronic capsules 20 and 21 ($B_4C_{20}N_8Ni_2$) are obtained by four B-atom dopings of 2, whereas capsule 22 ($B_8C_{16}N_8Ni_2$) is obtained by eight B-atom dopings of 2. Capsule 23 ($B_{12}C_{32}N_{14}Ni_2$) is obtained by 12 B and 6 N atom dopings of capsule 5.
- (8) Capsule 24 ($H_8C_{50}N_{10}FeNi$) contains Fe(II) and Ni(II). The octahedral coordination of Fe(II) is completed by the addition of a 2,2'-bipyridine (bpy) ligand.
- (9) Structures 25 (C_8N_8Ce) and 26 (C_8N_8Th) are Ce(IV) and Th(IV) encapsulated in the ligand of capsule 2. Cerium is smaller than thorium and displaced off the ligand center, whereas larger metal ions, such as U(IV), are too big to get encapsulated in this ligand.

These capsules can be extended by adding larger C atom cones that would elongate them and increase their diameter. One could also insert in them CNT segments that would elongate them. The capsule fusion rims can be designed to have zigzag or “armchair” structures.

IV. RESULTS AND DISCUSSION

We use Ni(II) in the capsule doping because it forms stable square planar and tetrahedral complexes. We treat the capsules in Fig. 1 as neutral in analogy to the Ni-doped nanocones.¹³ Capsules 1–4, 9, and 16–22 contain two Ni atoms and octadentate *capsule ligands* (CLs). Capsules 5, 6, and 23 contain two Ni atoms and hexadentate CLs. Capsule 7 contains two Ni atoms and a heptadentate CL, whereas capsule 8 contains a tetradentate CL. Capsules 10–16 contain from three to six metal atoms and multidentate CLs.

In Fig. 1, we organize these capsules in four structurally dissimilar groups labeled A–D. In group A [Fig. 1 (top panel)], we include capsules 1–7 that comprise the seven distinct capsule frameworks considered in this article. In group B [Fig. 1 (middle panel)], we include capsules 8–15 that are obtained by Ni doping of capsule 4. In group C [Fig. 1 (bottom panel)], we include capsules 16–23 that are obtained by B doping of capsules 2 and 5. In the last group D [Fig. 1 (bottom right panel)], we include capsules 24–26 that contain Fe-doping and encapsulated heavy metal ions.

We also study separately the CLs that are optimized as neutral molecules. This allows us to analyze the geometrical changes caused by the metal coordination and calculate the homolytic binding energies.

A. Ground electronic states in capsules

All capsules contain even number of electrons. The CLs also contain even number of electrons except for the CL of capsule 7. For structures that contain even number of electrons, we determine the *ground electronic state* as the state with the lowest total energy among the closed-shell singlet and the open-shell triplet, quintet, heptet, nonet, and endecet states. The ground electronic state of the CL of capsule 7 is determined as the state with the lowest total energy among the open-shell doublet, quartet, and sextet states. The ground state search is also aimed at the minimization of the percent spin contamination $\langle \Delta S^2 \rangle_{\text{cont}}$

$$\langle \Delta S^2 \rangle_{\text{cont}} = \frac{[\langle S^2 \rangle - S(S+1)]100}{[S(S+1)]}. \quad (1)$$

The $\langle S^2 \rangle_{\text{cont}}$ values are obtained as part of the geometry optimization output. For triplet, quartet, quintet, heptet, nonet, and endecet spin states, the S values of 1.00, 1.50, 2.00, 3.00, 4.00, and 5.00 yield $S(S+1)$ values of 2.00, 3.75, 6.00, 12.00, 20.00, and 30.00, respectively. A value of $\langle \Delta S^2 \rangle_{\text{cont}}$, which is lower than 10% (0.1) before spin annihilation should indicate that the spin contamination is negligible.⁴⁰ In our search of ground states, we apply a stricter criterion of $\langle \Delta S^2 \rangle_{\text{cont}} < 2\%$ before spin annihilation.

The results are listed in Table I. In group A, the ground state of the smallest capsule 1 is quintet, whereas the ground states of capsules 2–4 are singlet. In these four capsules, the Ni coordination is pseudo square-planar.¹³ For comparison,

TABLE I. Selected optimized distances (\AA) for neutral ligands $[\text{N-N(L)}]$ and complexes $[\text{N-N(cx)}, M\text{-N} (M=\text{metal atom}), \text{and } M\text{-M}]$, N-N-N-M dihedral angles (degrees) in their ground electronic states (GS). Mülliken metal atom charges ($q(M)$, e), Mülliken metal atom spin densities $[\text{Spin}(M), e]$, binding energy (E_b, eV), and HOMO-LUMO gaps (H-L, eV) for the neutral complexes in GS as well as lowest-lying excited state energies $[E \text{ (LLES)}]$. The GS and LLES types s, t, q, h, n , and ed are singlet, triplet, quintet, heptet, nonet, and endecet, respectively. The HOMO-LUMO gaps of open-shell systems are determined relative to LUMOs of the same spin type as the HOMOs. The N-N distances for capsules 1–4 and 7–22 are for N atoms *trans* to the Ni atom. The N-N distances for capsules 5, 6, 7 (top), and 23 are for N atoms that belong to the same metal coordination site. The ligand N-N distances are defined as in the corresponding complexes. For capsules 10, 10', and 12–15, only the diametric $M\text{-M}$ distances are listed. The dihedral N-N-N-M angles involve the N atoms bonded to the same metal atom.

Complex	GS	E (LLES)	Spin(M)	$q(M)$	N-N(L)	N-N(cx)	$M\text{-N}$	$M\text{-M}$	N-N-N-M	E_b	H-L
Group A											
1	q	0.21(t)	1.55	1.17	3.42	3.44	1.98	4.24	36.0	-5.90	2.61
2	s	0.15(t)	...	1.03	3.95	3.72	1.91	4.88	17.9	-8.51	1.55
3	s	0.09(t)	...	1.01	3.87	3.72	1.91	7.32	17.7	-8.94	1.09
4	s	0.12(t)	...	1.02	3.85	3.70	1.88	6.71	15.2	-7.73	1.00
5	h	0.05(q)	1.75	1.30	2.69	2.72	1.95	8.23	55.9	-12.40	0.94
6	q	0.29(h)	1.62	1.22	2.52	2.49	1.96	11.31	61.9	-11.38	1.15
7 (top)	t	0.33(q)	1.64	1.22	2.51	2.48	1.97	13.85	62.1	-11.55	1.11
7 (bottom)	t	0.33(q)	0.00	1.02	3.64	3.63	1.85	13.85	15.3	-9.53	1.11
Group B											
8	s	0.06(t)	...	1.02	3.85	3.71	1.89	...	15.3	-7.61	1.03
9	t	0.05(s)	0.02, 0.03	1.00, 1.01	3.80	3.70, 3.72	1.88	4.72	14.4, 14.9	-7.56	0.93
10	s	0.43(t)	...	1.02	3.81–3.84	3.71	1.89	6.56	14.6, 16.6	-7.79	1.34
10'	s	0.09(t)	...	1.01–1.02	3.81–3.83	3.71	1.89–1.90	7.20	14.4, 16.6	-7.59	1.09
11	t	0.09(q)	0.00–0.02	1.01–1.02	3.78–3.79	3.67–3.73	1.87–1.90	4.78–4.80	16.5	-7.44	1.05
12	s	0.13(t)	...	0.99–1.01	3.77–3.85	3.71, 3.72	1.89	6.34, 7.06	13.5, 16.3	-7.81	1.85
13	s	0.04(t)	...	1.00–1.02	3.77–3.74	3.67–3.72	1.88–1.90	6.73	14.1, 16.6	-7.55	1.33
14	s	0.07(t)	...	0.99–1.03	3.70–3.74	3.70, 3.71	1.89	6.51, 6.93	14.3, 15.6	-7.60	1.24
15	s	0.05(t)	...	0.98–1.00	3.69–3.73	3.71, 3.72	1.89	6.70, 6.79	16.5, 18.1	-7.48	1.10
Group C											
16 (top)	t	0.06(s)	0.02	1.03	4.54, 3.89	3.81, 3.77	1.94, 1.95	4.96	15.4–18.8	-9.41	1.17
16 (bottom)	t	0.06(s)	0.01	1.02	3.95	3.72	1.89–1.92	4.96	17.7–18.6	-9.41	1.17
17 (top)	s	0.32(t)	...	1.04	4.24, 4.14	3.77, 3.78	1.91, 1.95	4.90	17.1, 17.3	-9.16	1.56
17 (bottom)	s	0.32(t)	...	1.02	3.95	3.69–3.71	1.88–1.91	4.90	17.9, 18.4	-9.16	1.56
18	s	0.21(t)	...	1.03	4.12, 3.93	3.74, 3.72	1.92, 1.91	4.91	18.7	-9.48	1.54
19	s	0.01(t)	...	1.04	4.25, 3.84	3.72, 3.74	1.91, 1.90	4.91	16.9, 17.5	-8.89	1.22
20	s	0.10(t)	...	1.03	4.11, 4.21	3.76, 3.77	1.95, 1.92	4.99	16.9, 17.5	-9.24	1.21
21 (top)	s	0.12(t)	...	1.03	4.34	3.84	1.96	5.01	16.9	-10.25	1.90
21 (bottom)	s	0.12(t)	...	1.01	3.82	3.70	1.90	5.01	18.3	-10.25	1.90
22	t	0.06(s)	0.10	1.02, 1.03	4.41	3.75, 3.86	1.96, 1.92	4.95	15.1, 16.7	-9.99	1.45
23	ed	0.02(n)	1.87	1.31	2.89	2.88	1.90	8.27	48.2	-13.20	1.18
Group D											
24 (Ni)	q	0.23(h)	0.00	0.99	3.87	3.73	1.91	8.01	16.7	-8.94	1.16
24 (Fe)	q	0.23(h)	3.78	1.47	3.87	3.77	2.18	8.01	39.7	-12.15	1.16
25 (bottom)	s	0.15(t)	...	0.05	3.95	3.93	2.44–2.53	-7.92	1.35
26	s	0.14(t)	...	0.24	3.95	3.93	2.81–2.90	-9.67	1.57

the ground states of pure carbon fullerenes C_{20} and C_{60} in the I_h symmetry are singlet.^{41,42} The ground state of C_{36} in D_{6h} is triplet.⁴³ The ground states of capsules 5 and 6 are heptet and quintet, respectively. In these capsules, the Ni coordination is pseudotetrahedral.¹³ For comparison, the metal-doped nanocones, related to capsules 5 and 6, have quintet and quartet ground states, respectively.¹³ The ground state of capsule 7, related to capsules 4 and 6, is triplet. These results show that the ground state multiplicity of the metal-doped capsules increases as high-spin metal species (i.e., tetrahedral Ni) are introduced. The Ni-doped capsule ground state multiplicities are also higher than the respective cones.¹³

In group B, the ground states are singlet except for capsules 9 and 11 that have triplet ground states. This suggests that metal doping at adjacent sites could produce structures with higher ground state multiplicity. In group C, the ground states are singlet except for capsules 16 and 22 that have triplet ground states. The ground state of capsule 23 is endecet, suggesting that BN doping could be particularly effective for ground state tuning. In group D, the ground state of the bimetallic capsule 24 is quintet. Ground states with high multiplicity are typical for Fe(II) complexes because Fe(II) has small octahedral ligand-field splitting energy. The ground states of capsules 25 and 26 that contain a Th and a Ce atom,

respectively, are singlet. These results show that the ground state multiplicity of the metal and B-doped fullerenes depends strongly on the nature and organization of the dopants.

We now discuss the stability of metal- and boron-doped capsules by comparing their ground state energies. First, we consider the parent structure 4 and the Ni-doped capsules of group B. For two Ni atom dopings, capsule 9 is more stable than 4 by 0.16 eV. The three Ni atom dopings are in the three isomers 10, 10', and 11. In isomer 10, there are two Ni doping sites located on both sides of fused 6–6 rings, whereas in 10' there are two Ni doping sites located on both sides of a 5–5 junction. The ground state energies of isomers 10' and 11 are higher than those of isomer 10 by 0.65 and 0.59 eV, respectively. For four Ni atom dopings, capsule 12 is more stable than capsule 13 by 0.70 eV. These results suggest that the preferred Ni-doping mode is with the dopants far apart.

Second, we consider the B-doped capsules of group C. Capsule 18 is the most stable among capsules 16–19 that are doped with two B atoms. The energies of capsules 16, 17, and 19 are higher than that of capsule 18 by 0.13, 0.21, and 0.27 eV, respectively. These results suggest that the preferred B-doping mode is with two B atoms at *para* positions in the same six-membered ring. We use this result for the B-doping mode selection for capsule 22. In capsules 20 and 21, with four B atoms, the latter is more stable than the former by 0.11 eV.

The ground state spin contamination values for capsules 1, 5, 6, 7, 9, 11, 16, 22, 23, and 24 obtained before (after) spin annihilation are 6.03 (6.03), 12.05 (12.00), 6.03 (6.03), 2.03 (2.03), 2.09 (2.00), 2.06 (2.00), 2.03 (2.00), 2.02 (2.00), 30.08 (30.00), and 6.08 (6.07), respectively. These results show that the ground-state spin multiplicities are highly pure.

B. First excited electronic states in capsules

The lowest excited states for these capsules have been optimized during the ground state search. The results are only reliable when the energy separation is larger than the DFT accuracy threshold, estimated to be ≈ 0.1 eV (Ref. 44). In group A, the lowest-lying excited state energies are higher than the ground state energies by more than 0.1 eV except for capsule 5. The lowest-lying excited state of capsule 5 is impure ($\langle \Delta S^2 \rangle_{\text{cont}} = 18\%$).

In group B, the lowest-lying excited state energies of capsules 9 and 13–15 are higher than the ground states by 0.07 eV or less. These capsules contain adjacent Ni doping sites. In group C, capsule 19 has a particularly low-lying excited state. This capsule is the least stable isomer of capsules 16–19. For capsule 23, the $\langle \Delta S^2 \rangle_{\text{cont}}$ values of the endecet ground and nonet lowest-lying excited states are 0.3% and 5%, respectively. Our results show that the ground state of this structure would be mixed due to the small energy difference between these two states.

C. The electronic states in capsule ligands

The CL ground states are singlet except for capsules 5, 7, and 23 that have triplet, doublet, and nonet ground states, respectively. We also discuss the stability of the CLs. For the

CLs of capsule 4 and group B, the stability trends are rather different from the respective capsules. The CL of capsule 9 is more stable than that of capsule 4 by 0.56 eV, while the CL of capsule 11 is the most stable among the dodecadentate CLs. The energies of CLs 10 and 10' are higher than that of CL 11 by 0.47 and 0.51 eV, respectively. Of the two hexadecadentate CLs, capsule 13 is more stable than capsule 12 by 0.36 eV. This comparison shows that CLs containing larger complete fragments of C_{60} are more stable.

In group C, the most stable among the capsules that contain two B atoms is capsule 19. The energies of CLs 16, 17, and 18 are higher than that of CL19 by 0.96, 0.47, and 0.90 eV, respectively. Thus, the CL stability increases in the order of $16 < 18 < 17 < 19$, which is almost the opposite to that of the capsules, $19 < 17 < 16 < 18$. The energy of the CL of capsule 20 is higher than that of capsule 21 by 1.91 eV. Opposite stability trends for ligands and their complexes seem reasonable, considering that stable ligands would be less prone to structural changes upon complexation.

The lowest-lying excited states of the CLs of capsules 5, 7, and 23 are quintet, quartet, and heptet, and their energies are higher than the respective ground states by 0.18, 0.08, and 0.05 eV. The lowest-lying excited states of the rest of the capsules are triplet and their energies are higher than the singlet ground states by more than 0.2 eV.

D. The spin density in capsules

In Table I, we also list the Mülliken spin density at the metal atom in capsules. Generally, the Ni atom spin densities increase as the ground state multiplicities increase. However, the square-planar complexes tend to have lower Ni atom spin densities. Capsules 7 and 24 are highly spin polarized, as the spin density of one Ni atom in these structures is zero. The spin polarization effect in capsule 7 is achieved as a result of different Ni(II) coordination. In capsule 24, the spin polarization arises from doping with different metal atoms. The spin polarization of this structure can be additionally tuned by the attachment of paramagnetic ligands.⁴⁵ The presence of ground electronic states of high multiplicity together with the energetic closeness of states with different multiplicity suggests that one could easily spin polarize these systems and make them potentially useful for magnetic applications.⁴⁶

In Fig. 3, we show the electron spin density distribution for several capsules. The electron spin density is calculated as the difference between the α (spin-up) and β (spin-down) electron densities. In top left and middle, we show that extension of the B and N doping in capsule 23 leads to spreading of the spin density over larger part of the capsule relative to capsule 5. In top right, we show the strong spin polarization induced by the two different metal coordinations at the top and bottom of capsule 7. The presence of high-spin Fe(II) in capsule 24 also yields a highly spin-polarized structure.

E. The charge density in capsules

In Table I, we also list the Mülliken charges on the Ni atom in capsules. In general, the Ni atom charge increases as the ground state multiplicity increases. Consequently, the tet-

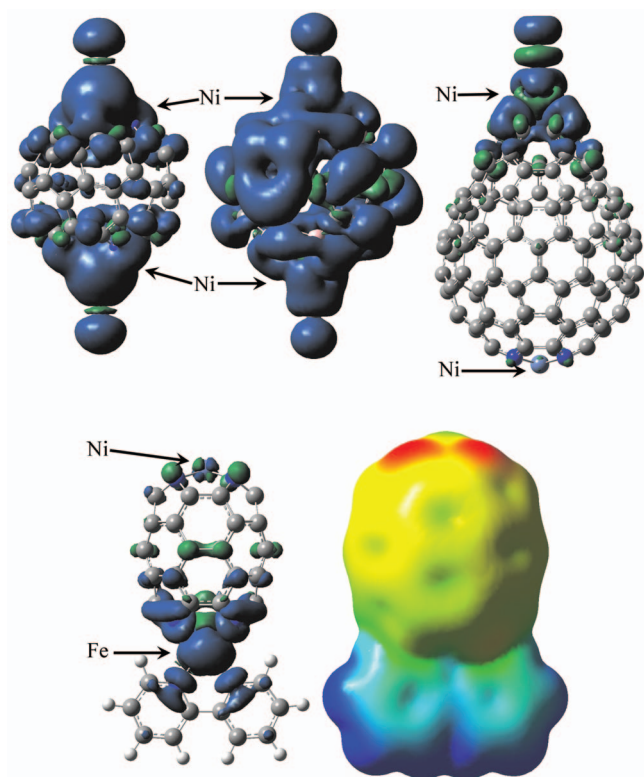


FIG. 3. (Color) Electron spin density surface ($\pm 0.0004 e/\text{bohr}^3$) of capsules 5 (top left), 23 (top middle), 7 (top right), and 24 (bottom left). Electrostatic potential of capsule 24 in the interval $(-0.04, +0.04) e$ mapped on the $0.0004 e/\text{bohr}^3$ total electron density surface (bottom right).

rahedral Ni sites have higher Ni atom charges than the square-planar Ni sites. For capsules 1–4, the Ni atom charge increases as the Ni–N distance increases. It is particularly interesting to see the extensive charge polarization in the asymmetric capsule 7, caused by the different coordination environment. In group B, increased Ni doping causes small charge decrease, as the charge is distributed over several Ni atoms. In group C, increased B atom doping causes small increase in the Ni atom charge. The largest metal atom charge is obtained for the Fe atom of capsule 24. This structure is highly charge polarized, as shown in Fig. 3 (bottom right). The smallest metal atom charge is obtained for Ce encapsulated in capsule 25.

F. Geometry optimization

Geometry optimization with DFT of N-doped CNTs has shown that substitutions of C with N atoms lead to less than 0.02 \AA shifts in the atomic positions.^{12,47} In Table I, we list selected structural parameters obtained from the ground-state geometry optimization of the capsules shown in Fig. 1, and the related anionic CLs. Our results are obtained with the B3LYP functional, which is successful in accounting for the relative changes in metal-ligand bond lengths.³³ Due to their extended π -structures, the CLs are rigid and undergo smaller geometrical changes upon metal coordination relative to the respective nanocones,¹³ mostly observable at the N atom positions. These changes can be quantitatively evaluated from the relative changes in the N–N distance *trans* to the Ni atom.

In group A, the N–N distance upon Ni coordination in capsule 1 increases by 0.6%. The N–N distance for capsule 2 decreases from 3.95 \AA for the ligand to 3.72 \AA for the complex, i.e., by 6.2%. The relative changes in the N–N distance for capsules 3 and 4 are 4.0 and 4.1%, respectively. For capsule 5, the N–N distance increases by 1.1%, whereas for capsule 6 it decreases by 1.2%. The capsules and CLs have shorter N–N distances in comparison to the metal-doped nanocones and nanocone ligands.¹³ This arises from the increased rigidity of the capsules relative to the cones.

In group C, we list two N–N distances in Table I. The first value is for the N–N distance that involves an N atom adjacent to a B doping site, whereas the second value is for the N–N distance that does not involve an N atom directly bonded to B atom(s). For two B atom dopings near one N atom, the N–N distances of the same coordination site change the most, as we show for capsule 16 (top). The N–N distances that do not involve N atoms adjacent to B are the same as in capsule 2, as we list for capsules 16, 17, and 21 (bottom). For capsule 23, the B and N doping causes N–N distance elongation of 0.16 \AA relative to capsule 5. This structural relaxation is large in comparison to CNTs.^{12,47}

In group D, the N–N distance for capsule 24 at the Fe atom is longer than at the Ni atom because of the larger ionic radius of high-spin Fe(II) relative to zero-spin Ni(II). For capsules 25 and 26, the N–N distance is longer than for capsule 2.

We also study the metal-N (*M*-N) bond lengths and N–N–N–*M* torsion angles in these complexes and present the results in Table I. The longest Ni–N bond is obtained for capsule 1 because this structure contains strained four-membered NiNNC rings. The Ni–N bond length is not affected by elongation of the capsule from 2 to 3. For capsules 5, 6, and 7 (top), we note a small Ni–N bond elongation. The Ni–N bond in capsule 7 (bottom) is shorter than that in capsule 4. This is due to the specific capsule fusion mode that causes contraction of the bottom coordination site. In group B, the Ni–N bond lengths show small variations.

In group C, B doping causes large Ni–N bond elongation. This effect is most pronounced for capsule 16, 17, and 21, where the B atoms are concentrated near one or several N atoms. This concentration of doping sites in the vicinity of N atoms causes elongation of the nearest Ni–N bond. For capsules 18–20 and 22, we list two Ni–N bond length values. The first value is for N atoms adjacent to the B-doping site and the second value is for the other cases. An interesting effect occurs in capsule 22, where the eight B atom doping causes steric strain that is relaxed by elongation of one pair of Ni–N in *trans* position relative to Ni and shortening of the other. For capsule 23, the B and N doping causes shortening of the Ni–N bonds by 0.05 \AA .

In group D, the Fe–N(bpy) bond length for capsule 24 is 2.25 \AA . This Fe–N bond length is typical for high-spin Fe(II) complexes.⁴⁸ For capsule 25, the Ce atom is displaced off the CL center because this atom is too small to be effectively encapsulated. The Ce–N bond lengths are comparable to 2.47 \AA obtained by x-ray adsorption near-edge structure determination for the bis(naphthalocyanato) cerium complex.⁴⁹ For capsule 26, the Th atom is almost at the

center of the CL, indicating a very effective encapsulation. The Th–N bond lengths in the range of 2.71–2.80 Å are reported from x-ray crystallography.⁵⁰

The N–N–N–M torsion angle is useful for evaluation of the metal atom displacement relative to the plane of the coordinating N atoms. For pseudo-square-planar complexes, large values of the torsion angle suggest high structural strain and reduced stability. The largest torsion angle of all square-planar structures is obtained for the smallest capsule 1, indicating that this structure is highly strained. The torsion angles for capsules 2 and 3 are larger than that of capsule 4 by 2°, suggesting that the former are more strained than the latter. For capsule 6, the torsion angle increases by 6° relative to capsule 5, as the capsule diameter and the N–N(cx) (cx denotes complex) distance decrease. In group B, the torsion angle increases as the amount of Ni doping increases. The extensive B and N doping in capsule 23 causes the torsion angle to decrease relative to capsule 5. For capsule 24, the Fe atom torsion angle is large because of the pseudo-octahedral coordination.

The Ni–C bond lengths for capsules 5, 6, 7, and 23 are 1.90, 1.94, 1.95, and 1.93 Å, respectively. For capsules 5–7, the Ni–C bonds are shorter than the respective Ni–N bonds, whereas for the B-doped capsule 23 the Ni–C bonds are longer than the Ni–N. For capsule 25, the Ce–C bond lengths (C atoms bonded to the bottom N atoms, Fig. 1) are 2.53–2.54 Å. It is particularly interesting to consider the Th atom encapsulation in capsule 26. The Th–C(six-membered ring) bonds of 2.70–2.80 Å are shorter than the Th–N bonds but longer than 2.61 Å reported for Th–C(CO).⁵¹

G. Metal-ligand binding energies

The metal-ligand bond dissociation energies provide crucial information about the capsule stability. We calculate these energies for homolytic (E_b) dissociation, i.e., dissociation yielding neutral metal atoms and ligands,

$$E_b = [E(n) - E(\text{CL}) - E(M) - E(\text{CN})]/m. \quad (2)$$

Here, $E(n)$ is the total energy of capsule n , $E(\text{CL})$ is the total energy of the neutral singlet CL, $E(M)$ is the total energy of all *isolated* metal atoms in the singlet state, $E(\text{CN})$ is the energy of the doublet CN^0 , and m is the number of metal atoms in the capsule. The E_b energies are obtained per metal coordination site, except for the asymmetric capsules 7 and 24, where we calculate E_b for each metal atom separately. The binding energy of the Ni atom at the top of capsule 7 is $E_b(\text{Ni}(7_{\text{top}})) = E(n) - E(\text{CL} + \text{Ni}_{\text{bottom}}) - E(\text{Ni}) - E(\text{CN})$, where $E(\text{CL} + \text{Ni}_{\text{bottom}})$ is the total energy of the structure that contains the CL of capsule 7 and the bottom Ni atom, optimized in doublet state. Similarly, binding energy of the N atom at the bottom of capsule 7 is $E_b(\text{Ni}(7_{\text{bottom}})) = E(n) - E(\text{CL}) - 2E(\text{Ni}) - E_b(\text{Ni}(7_{\text{top}})) - E(\text{CN})$. The binding energy of the Fe atom at the bottom of capsule 24 is $E_b(\text{Fe}) = E(n) - E(\text{CL}) - E(\text{Ni}) - E(\text{Fe}) - E_b(\text{Ni}(3)) - E(\text{bpy})$, where $E(\text{Fe})$ is the total energy of a singlet Fe atom, $E_b(\text{Ni}(3))$ is the binding energy of Ni in capsule 3, and $E(\text{bpy})$ is the total energy of a neutral singlet bpy ligand. The capsule and ligand energies are obtained for the optimized geometries of the structures.

Thus, the energy changes arising from the changes in geometry that occur as a result of the bonding are included in the homolytic bond dissociation energy.

The E_b values are listed in Table I. Low negative E_b values indicate strong metal-ligand bonds. In group A, the binding energy of capsule 1 is the highest because of its strained geometry. The E_b value of capsule 3 is lower than that of capsule 2, suggesting that capsule elongation relieves strain. The E_b value of capsule 4 is rather high, considering that the torsion angle does not suggest large strain. It could arise from a large geometry rearrangement upon Ni coordination and/or short N–N distances that do not allow for effective Ni coordination. The binding energies of capsules 5 and 6 that contain hexadentate CLs are lower than those of capsules 1–4. The stronger binding in capsule 5 relative to 6 is supported by the shorter Ni–N bond and the smaller torsion angle that is closer to the perfect tetrahedron value of 35.3°. In the asymmetric capsule 7, the E_b for the top Ni atom is lower than that for the bottom one by 2 eV. In this structure, the top and bottom Ni atom binding energies are lower than these of capsules 6 and 4, respectively, which have analogous coordination sites. The stronger binding in the asymmetric structure 7 could be due to strain relief at the fusion area.

In group B, the binding is weaker for structures that contain Ni atoms close together, as in capsules 9, 11, and 13, relative to 4, 10, and 12. This trend is supported by the capsule stability as evaluated from the total energies. Additional Ni doping also increases the binding strength.

In group C, the binding is stronger than for the undoped capsule 2. Increased B dopings for capsules 21 and 22 lead to increased Ni binding strength relative to capsules 16–20. Also, B doping near one Ni atom for capsules 16 and 21 increases the binding strength relative to capsules 17 and 20, respectively. For capsule 23, both B and N doping decrease the binding energy by 0.80 eV relative to the undoped capsule 5.

In group D, the high Fe atom binding strength for capsule 24 is due to its octahedral coordination. The Th binding energy for capsule 26 is higher than that for capsule 25. Our results for U, Th, and Ce encapsulation in the CL of capsule 2 show that this CL is particularly effective for Th binding and could be used for selective Th(IV) sequestration. For capsules 2–6, the E_b values show that the Ni-CL bond is weaker than the Ni-cone bonds reported previously.¹³ This is because the capsules are more rigid than the respective cones.

H. The highest occupied molecular orbital–lowest unoccupied molecular orbital energy gap

The energy gap between the highest occupied molecular orbital (HOMO) and the lowest unoccupied molecular orbital (LUMO) is an important characteristic of the stability of the ground electronic state. The HOMO-LUMO gap decreases upon capsule elongation from 2 to 3, similar to cone elongation.¹³ In group B, metal doping increases the energy gap, especially if the Ni atoms are not clustered together, as for capsules 10 and 12. In group C, B doping increases the HOMO-LUMO gap only if the doping sites are close to-

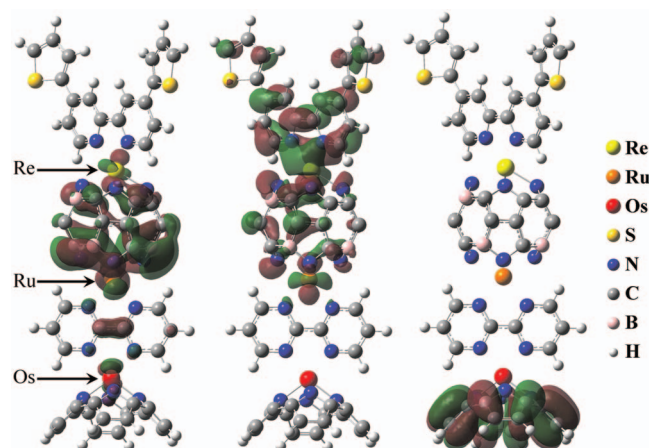


FIG. 4. (Color) (left) Frontier molecular orbitals HOMO-2, (middle) HOMO, and (right) LUMO of a sandwichlike light-harvesting antenna.

gether, as in capsules 16 and 21. The extensive BN doping of capsule 23 increases the energy gap by only 0.03 eV. In group D, the Fe atom doping of capsule 24 leads to 0.07 eV increase in the energy gap relative to capsule 3. For capsule 26, the energy gap is larger by 0.22 eV relative to capsule 25. The wider energy gap and the lower E_b value of capsule 26 indicate more stable structure relative to capsule 25. In groups B and C, the doping modes that lead to the formation of more stable structures also lead to large energy gaps.

V. APPLICATIONS

The above studies show that we can introduce various metallic binding sites into carbon nanostructures with minimal structural changes. The coordination sites can be finely tuned by the nature of the transition metal and the location of the doping site. The multiple binding sites can be functionalized in various patterns, especially when the capsules are extended into nanotubes. These metal-doped and functionalized nanosystems might show chemical, electronic, optical, and mechanical activity.

As a first example, we show in Fig. 4 the HOMO-2 (next nearest to the HOMO), HOMO, and LUMO diagrams for a *light-harvesting antenna* ($\text{H}_{26}\text{B}_5\text{C}_{61}\text{N}_{18}\text{S}_2\text{RuReOs}$). In order to spatioenergetically separate its active quantum states, we order the metals so that the polyimine moieties have decreasing metal-to-ligand charge transfer state energies, from Re(I) and Ru(II) to Os(II).⁵² Therefore, the system is formed by a cone¹³ containing an Os(II) atom on the tip that is coordinated to a 2,2'-bipyrimidine (bpm) ligand.⁵³ The latter is coordinated at the top to the Ru(II)-doped tip of a capsule derived from 21, while the other tip of the capsule is doped with a Re(I) atom coordinated to a 4,4'-dithiopheno-2,2'-bipyridine (dtbpy) ligand. The capsule of this closed-shell neutral antenna contains four B atoms as in capsule 21 and one B atom in *para* position. The B-doping mode of capsule 21 is selected because it yields the largest HOMO-LUMO gap in series C (Table I). The B atom doping at the *para* position yields the most stable structure among capsules 16–19.

This sandwiched system allows large *spatial* separation of its frontier orbitals, necessary in photovoltaic

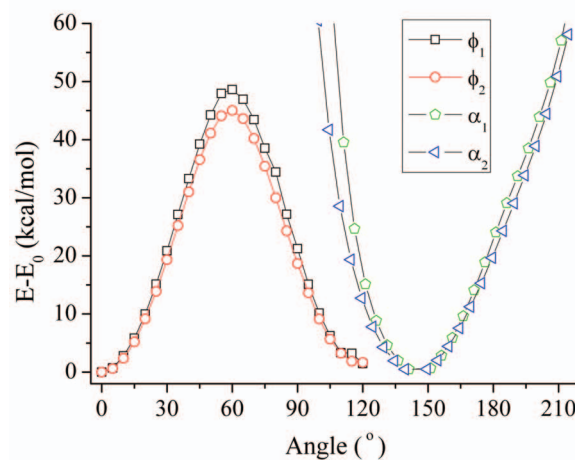
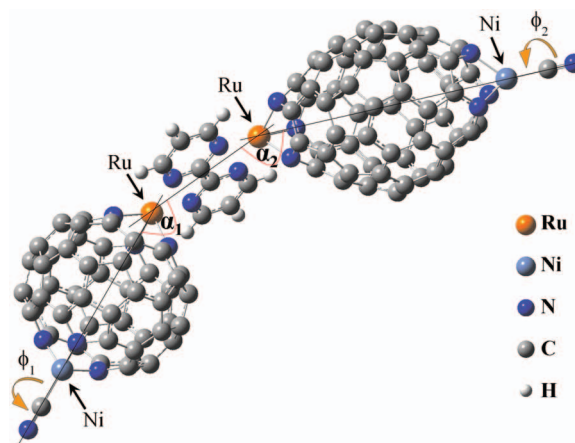


FIG. 5. (Color) (top) A nanomechanical system formed by two extended capsules coordinated to a bpm ligand. The system can be displaced from its equilibrium bent conformation by bending and twisting. (bottom) The relative energy of the nanomechanical system for twisting and bending. The E and E_0 are the total energies of the bent (twisted) and optimized structures, respectively.

conversion.⁵⁴ Its HOMO-LUMO energy gap is 1.38 eV, and the energy of the HOMO-2 is 0.21 eV lower than the HOMO. The B doping and thiophene covalent bonding increase the HOMO-LUMO gap by ≈ 0.8 eV, shifting it near the visible light range relative to the structure that contains capsule 2 and bpy. Chen *et al.*⁵⁵ showed that the electron-rich thiophene moiety covalently bonded to bpy increases the HOMO-LUMO gap of Ru(II) photosensitizers. The light-induced electronic transitions can occur from the HOMO and HOMO-2 that contain large Re-dtbpy and Ru-capsule orbital contributions, respectively, to the LUMO. The latter is strongly localized on the carbon part of the nanocone¹³ and should allow efficient charge collection at the electrode. The system is also highly rigid, preventing thus parasitic effects, such as electron tunneling.

As a second example, we present in Fig. 5 (top) a *nanomechanical system* ($\text{H}_6\text{C}_{118}\text{N}_{18}\text{Ni}_2\text{Ru}_2$), formed by two bimetallic capsules 5 and 6, having two Ru and two Ni atoms, coordinated via a bridging tetradentate bpm ligand. (We use the fourth period d^6 Ru atoms instead of d^8 Ni atoms because the former can better accommodate the five-coordinate ligand environment.) The ground state of this structure is a

heptet and its energy gap is 0.68 eV. The equilibrium bending of the structure is caused by different symmetries of the capsules (threefold) and the ligand (twofold) around the two Ru atoms as well as by the different capsule coordination sites. In a series of single-point calculations, we calculate the energies of bending about angles α_1 and α_2 , as well as twisting (spinning) about angles ϕ_1 and ϕ_2 . The spinning axes for ϕ_1 and ϕ_2 are defined as the median lines for the lower left and upper right capsules (inclusive of Ru, Ni, and CN), respectively. The bending for α_1 and α_2 is done in the plane defined by the Ni atoms at the bottom left and top right, respectively, as well as the two Ru atoms. In the optimized structure, the values of α_1 and α_2 are 146.2° and 144.5°, respectively. The angles are varied one at a time, while the rest of the structure remains unchanged.

In Fig. 5 (bottom), we show the dependence of the system total energy on the twisting and bending angles, where the zero values of ϕ_1 and ϕ_2 correspond to the optimized structure. The ϕ_1 -angle twisting barrier is higher than the ϕ_2 -barrier by 5.0 kcal/mol. The bending energy dependence shows that the system is more rigid with respect to angle α_1 than α_2 . The system is more rigid toward decreasing α_1 and α_2 than toward increasing them relative to the optimized values. The complex resembles a joint in arms or legs and might be used in nanomechanics.

VI. CONCLUSIVE NOTES

We have investigated metal, nitrogen, and boron doping in carbon nanocapsules structurally related to fullerenes. The results can be summarized as follows. (1) Nickel atom doping of fullerenes yields capsules with binding energies comparable to Ni(II)-doped nanocones and Ni(II) porphyrin. These capsules provide a wide range of possibilities for binding of functional groups. (2) The ground state spin multiplicities of these capsules increase as the buckling of the NiN₄ moiety increases. The presence of low-lying excited states allows for reactivity control in analogy to natural metalloporphyrins, where spin state changes are one of the most prominent features.⁵⁶ (3) The preferred metal doping patterns contain metal atoms that are not in close proximity. (4) The preferred B-doping sites have B atoms separated by two C atoms. Additional B and N doping increases the ground state spin multiplicity, binding energy and HOMO-LUMO gap, thus increasing capsule stability. (5) The CLs can selectively encapsulate heavy metal ions. For the CL that is structurally related to C₃₆, Th(IV) forms the most effective bonding, suggesting that these structures could be used as size-selective sequestration agents. (6) The capsules presented could be used in multifunctional devices, such as nanomagnets, light-harvesting antenna, and nanomechanical systems. The transition metal pseudo-square-planar sites built in these capsules can act as catalysts, as it has been realized on walls of CNTs (Ref. 17) and on metcars.²⁹

The described metal-doped carbon nanostructures might be experimentally realized with advanced chemical methods, allowing substitutions of selected carbon atoms or via a direct stepwise synthesis. In the first step of such a synthetic approach, one could prepare an open capsule with nitroge-

nated rim. The opening can be realized by electron beam cutting or by etching in solution.⁵⁷ The subsequent nitroge-nation can be done by using transient arc discharge.⁵⁸ In the second step, we could coordinate the transition metal atom to the nitrogenated rim. More refined structures might be possible to prepare in a series of ring closure reactions in analogy to the synthetic schemes of C₆₀.⁵⁹ The chemical vapor deposition method of Yang *et al.*¹⁷ for the preparation of FeN₄ catalytic site built-in CNT walls could be extended to fullerenes. These systems form a bridge between traditional nanostructures and molecules encountered in organic chemistry and biochemistry. As such, they should be of large interest for their potential role in the future nanodevices.

ACKNOWLEDGMENTS

This work was partially supported by the National Computational Science Alliance (NCSA) and the National Energy Research Scientific Computing Center (NERSC).

- ¹H. W. Kroto, J. R. Heath, S. C. O'Brien, R. F. Curl, and R. E. Smalley, *Nature (London)* **318**, 162 (1985); C. Piskoti, J. Yarger, and A. Zettl, *ibid.* **393**, 771 (1998); H. Prinzbach, A. Weller, P. Landerberger, F. Wahl, J. Worth, L. Scott, M. Gelmont, D. Olevano, and B. von Issendorff, *ibid.* **407**, 60 (2000).
- ²S. Lijima, T. Ichihashi, and Y. Ando, *Nature (London)* **356**, 776 (1992).
- ³M. Ge and K. Sattler, *Chem. Phys. Lett.* **220**, 192 (1994); A. Krishnan, E. Dujardin, M. Treacy, J. Hugdahl, S. Lynum, and T. Ebbesen, *Nature (London)* **388**, 451 (1997).
- ⁴M. S. Dresselhaus, G. Dresselhaus, and P. C. Eklund, *Science of Fullerenes and Carbon Nanotubes* (Academic, San Diego, 1996).
- ⁵N. G. Chopra, R. J. Luyken, K. Cherry, V. H. Crespi, M. L. Cohen, S. G. Louie, and A. Zettl, *Science* **269**, 966 (1995).
- ⁶T. Oku, T. Kusunose, T. Hirata, R. Hatakeyama, N. Sato, K. Niihara, and K. Suganuma, *Diamond Relat. Mater.* **9**, 911 (2000).
- ⁷P. Král, E. J. Mele, and D. Tománek, *Phys. Rev. Lett.* **85**, 1512 (2000); E. J. Mele and P. Král, *ibid.* **88**, 056803 (2002).
- ⁸M. Zheng, A. Jagota, M. S. Strano, A. P. Santos, P. Barone, S. G. Chou, B. A. Diner, M. S. Dresselhaus, R. S. Mclean, G. B. Onoa, G. G. Samsonidze, E. D. Semke, M. Usrey, and D. J. Walls, *Science* **302**, 1545 (2003).
- ⁹S. Banerjee, T. Hemraj-Benny, and S. S. Wong, *Adv. Mater. (Weinheim, Ger.)* **17**, 17 (2005).
- ¹⁰S. S. Wong, E. Joselevich, A. Woolley, C. Cheung, and C. Lieber, *Nature (London)* **394**, 52 (1998).
- ¹¹N. W. S. Kam, T. C. Jessop, P. A. Wender, and H. Dai, *J. Am. Chem. Soc.* **126**, 6850 (2004).
- ¹²C. P. Ewels and M. J. Glerup, *J. Nanosci. Nanotechnol.* **5**, 1345 (2005).
- ¹³S. R. Stoyanov and P. Král, *J. Phys. Chem. B* **110**, 21480 (2006).
- ¹⁴S. R. Stoyanov, P. Král, and B. Wang, *Appl. Phys. Lett.* **90**, 153110 (2007).
- ¹⁵M. Terrones, P. M. Ajayan, F. Banhart, X. Blase, D. L. Carroll, J.-C. Charlier, R. Czerw, B. Foley, N. Grobert, R. Kamalakaran, P. Rohler-Redlich, M. Rühle, T. Seeger, and H. Terrones, *Appl. Phys. A: Mater. Sci. Process.* **74**, 355 (2002).
- ¹⁶M. Lefèvre, J. P. Dodelet, and P. Bertrand, *J. Phys. Chem. B* **106**, 8705 (2002); F. Jaouen, S. Marcotte, J. P. Dodelet, and G. Lindbergh, *ibid.* **107**, 1376 (2003).
- ¹⁷J. Yang, D.-J. Liu, N. N. Kariuki, and L. X. Chen, *Chem. Commun. (Cambridge)* **2008**, 329.
- ¹⁸W. Vielstich, A. Lamm, and H. Gasteiger, *Handbook of Fuel Cells: Fundamentals, Technology, Applications* (Wiley, Chichester, UK, 2003), Vol. 2.
- ¹⁹M. Matsubara and C. Massobrio, *Mater. Sci. Eng., C* **26**, 1224 (2006).
- ²⁰J. F. Christian, Z. Wan, and S. L. Anderson, *J. Phys. Chem.* **96**, 10597 (1992); U. Reuther and A. Hirsch, *Carbon* **38**, 1539 (2000); F. Fulop, A. Rockenbauer, F. Simon, S. Pekker, L. Korecz, S. Garaj, and A. Janossy, *Chem. Phys. Lett.* **334**, 233 (2001).
- ²¹J. Q. Hou and H. S. Kang, *J. Phys. Chem. A* **111**, 1111 (2007).
- ²²J. Cioslowski, *Electronic Structure Calculations on Fullerenes and their*

- Derivatives* (Oxford University Press, New York, 1995).
- ²³ R. W. Alder, J. N. Harvey, P. von R. Schleyer, and D. Moran, *Org. Lett.* **3**, 3233 (2001).
- ²⁴ J. Pattanayak, T. Kar, and S. Sheiner, *J. Phys. Chem. A* **108**, 7681 (2004).
- ²⁵ B. C. Guo, K. P. Kerns, and A. W. Castleman, *Science* **255**, 1411 (1992).
- ²⁶ B. C. Guo, P. Wei, J. Purnell, S. A. Buzza, and A. W. Castleman, *Science* **256**, 515 (1992).
- ²⁷ J. M. Lightstone, H. Mann, M. Wu, P. M. Johnson, and M. G. White, *J. Phys. Chem. B* **107**, 10359 (2003).
- ²⁸ C. Zhang, W. Sun, and Z. Cao, *J. Chem. Phys.* **126**, 144306/1 (2007).
- ²⁹ P. Liu, J. M. Lightstone, M. J. Patterson, J. A. Rodriguez, J. T. Muckerman, and M. G. White, *J. Phys. Chem. B* **110**, 7449 (2006).
- ³⁰ K. S. Troche, V. R. Coluci, R. Rurali, and D. S. Galvao, *J. Phys.: Condens. Matter* **19**, 236222 (2007).
- ³¹ H. Shinohara, *Rep. Prog. Phys.* **63**, 843 (2000).
- ³² H. Lee, H. Kim, S.-J. Kahng, G. Kim, Y.-W. Son, J. Ihm, H. Kato, Z. W. Wang, T. Okazaki, H. Shinohara, and Y. Kuk, *Nature (London)* **415**, 1005 (2002).
- ³³ J. H. Rodriguez, D. E. Wheeler, and J. K. McCusker, *J. Am. Chem. Soc.* **120**, 12051 (1998); S. R. Stoyanov, J. M. Villegas, A. J. Cruz, L. L. Lockyear, J. H. Reibenspies, and D. P. Rillema, *J. Chem. Theory Comput.* **1**, 95 (2005).
- ³⁴ M. J. Frisch, G. W. Trucks, H. B. Schlegel *et al.*, GAUSSIAN 03, Revision C.02, Gaussian, Inc., Wallingford, CT, 2004.
- ³⁵ A. D. McLean and G. S. Chandler, *J. Chem. Phys.* **72**, 5639 (1980); R. Krishnan, J. S. Binkley, R. Seeger, and J. A. Pople, *ibid.* **72**, 650 (1980).
- ³⁶ M. Dolg, U. Wedig, H. Stoll, and H. Preuss, *J. Chem. Phys.* **86**, 2123 (1987); D. Andrae, U. Haussermann, M. Dolg, H. Stoll, and H. Preuss, *Theor. Chim. Acta* **77**, 123 (1990).
- ³⁷ G. te Velde, F. Bickelhaupt, S. Van Gisbergen, C. Guerra, E. Baerends, J. Snijders, and T. Ziegler, *J. Comput. Chem.* **22**, 931 (2001); C. Guerra, J. Snijders, G. te Velde, and E. Baerends, *Theor. Chem. Acc.* **99**, 391 (1998); ADF2004, 01, SCM, Theoretical Chemistry, Vrije Universiteit: Amsterdam, The Netherlands, <http://www.scm.com>.
- ³⁸ I. Narita and T. Oku, *Diamond Relat. Mater.* **12**, 1146 (2003).
- ³⁹ D. P. Rillema, R. Sahai, P. Matthews, A. K. Edwards, R. J. Shaver, and L. Morgan, *Inorg. Chem.* **29**, 167 (1990).
- ⁴⁰ D. C. Young, *Computational Chemistry: A Practical Guide for Applying Techniques to Real World Problems* (Wiley, New York, NY, 2001), pp. 227–228.
- ⁴¹ Z. Y. Wang, K. H. Su, H. Q. Fan, L. D. Hu, X. Wang, Y. L. Li, and Z. Y. Wen, *Comput. Mater. Sci.* **40**, 537 (2007).
- ⁴² B. Paulus, *Phys. Chem. Chem. Phys.* **5**, 3364 (2003).
- ⁴³ L. F. Yuan, J. Yang, K. Deng, and Q. S. Zhu, *J. Phys. Chem. A* **104**, 6666 (2000); M. N. Jagadeesh and J. Chandrashakhar, *Chem. Phys. Lett.* **305**, 298 (1999).
- ⁴⁴ M. Neurock, *J. Catal.* **216**, 73 (2003).
- ⁴⁵ T. Kalai, B. Bogнар, J. Jeko, and K. Hideg, *Synthesis* **15**, 2573 (2006); D. A. Shultz, *Polyhedron* **20**, 1627 (2001).
- ⁴⁶ T. Kambe, K. Kajiyoshi, M. Fujiwara, and K. Oshima, *Phys. Rev. Lett.* **99**, 177205 (2007).
- ⁴⁷ J.-Y. Yi and J. Bernholc, *Phys. Rev. B* **47**, 1708 (1993).
- ⁴⁸ J. Simaan, S. Poussereau, G. Blondin, J.-J. Girerd, D. Defaye, C. Philouze, J. Guilhem, and L. Tchertanov, *Inorg. Chim. Acta* **299**, 221 (2000).
- ⁴⁹ Z. Y. Wu, Y. Tao, M. Bnefatto, D. C. Xian, and J. Z. Jiang, *J. Synchrotron Radiat.* **12**, 98 (2004).
- ⁵⁰ R. J. Barton, R. W. Dabeka, H. Szengzhi, L. M. Mihichuk, M. Pizzey, B. E. Robertson, and W. J. Wallace, *Acta Crystallogr. C: Cryst. Struct. Commun.* **39**, 714 (1983).
- ⁵¹ P. G. Edwards, M. B. Hursthouse, K. M. A. Malik, and J. S. Parry, *J. Chem. Soc., Chem. Commun.* **10**, 1249 (1994).
- ⁵² V. Balzani, A. Juris, and M. Venturi, *Chem. Rev. (Washington, D.C.)* **96**, 759 (1996); S. R. Stoyanov, J. M. Villegas, and D. P. Rillema, *Inorg. Chem.* **41**, 2941 (2002).
- ⁵³ J. Collman, J. McDevitt, G. Yee, C. Leidner, L. McGullough, W. Little, and J. Torrance, *Proc. Natl. Acad. Sci. U.S.A.* **83**, 4581 (1986).
- ⁵⁴ G. J. Meyer, *Inorg. Chem.* **44**, 6852 (2005).
- ⁵⁵ C.-Y. Chen, S.-J. Wu, C.-G. Wu, J.-G. Chen, and K.-C. Ho, *Angew. Chem., Int. Ed.* **45**, 5822 (2006).
- ⁵⁶ M. Ravikanth and T. K. Chandrashekar, *Struct. Bonding (Berlin)* **82**, 105 (1995); R. Huber, *Eur. J. Biochem.* **187**, 283 (1990); M. Zimmer and R. H. Crabtree, *J. Am. Chem. Soc.* **112**, 1062 (1990).
- ⁵⁷ S. Wong, A. Woolley, E. Joselevich, and C. Lieber, *Chem. Phys. Lett.* **306**, 219 (1999).
- ⁵⁸ F. Banhart, J. Li, and M. Terrones, *Small* **1**, 953 (2005); K. Ziegler, Z. Gu, J. Shaver, Z. Chen, E. L. Flor, D. J. Schmidt, C. Chan, R. H. Hauge, and R. E. Smalley, *Nanotechnology* **16**, S539 (2005).
- ⁵⁹ K. Komatsu, M. Murata, and Y. Murata, *Science* **307**, 238 (2005); L. Scott, M. M. Boorum, B. J. McMahon, S. Hagen, J. Mack, J. Blank, H. Wegner, and A. de Meijere, *ibid.* **295**, 1500 (2002); Y. Rubin, T. Jarosson, G.-W. Wang, M. D. Bartberger, K. N. Houk, G. Schick, M. Saunders, and R. J. Cross, *Angew. Chem., Int. Ed.* **40**, 1543 (2001).